

Bounded Quadrant System: Error-bounded Trajectory Compression on the Go

[†]Jiajun Liu [†]Kun Zhao [†]Philipp Sommer

*Shuo Shang [†]Brano Kusy [†]Raja Jurdak

[†]AS Program, CSIRO, Pullenvale, Australia

{jiajun.liu, kun.zhao, philipp.sommer, raja.jurdak, brano.kusy}@csiro.au

*China University of Petroleum, Beijing, China

sshang@cup.edu.cn

Abstract—Long-term location tracking, where trajectory compression is commonly used, has gained high interest for many applications in transport, ecology, and wearable computing. However, state-of-the-art compression methods involve high space-time complexity or achieve unsatisfactory compression rate, leading to rapid exhaustion of memory, computation, storage and energy resources. We propose a novel online algorithm for error-bounded trajectory compression called the Bounded Quadrant System (BQS), which compresses trajectories with extremely small costs in space and time using convex-hulls. In this algorithm, we build a virtual coordinate system centered at a start point, and establish a rectangular bounding box as well as two bounding lines in each of its quadrants. In each quadrant, the points to be assessed are bounded by the convex-hull formed by the box and lines. Various compression error-bounds are therefore derived to quickly draw compression decisions without expensive error computations. In addition, we also propose a light version of the BQS version that achieves $\mathcal{O}(1)$ complexity in both time and space for processing each point to suit the most constrained computation environments. Furthermore, we briefly demonstrate how this algorithm can be naturally extended to the 3-D case.

Using empirical GPS traces from flying foxes, cars and simulation, we demonstrate the effectiveness of our algorithm in significantly reducing the time and space complexity of trajectory compression, while greatly improving the compression rates of the state-of-the-art algorithms (up to 47%). We then show that with this algorithm, the operational time of the target resource-constrained hardware platform can be prolonged by up to 41%.

I. INTRODUCTION

Location tracking is increasingly important for transport, ecology, and wearable computing. In particular, long-term tracking of spatially spread assets, such as wildlife [1], augmented reality glasses [2], or bicycles [3] provides high resolution trajectory information for better management and services. For smaller moving entities, such as flying foxes [4] or pigeons [5], the size and weight of tracking devices are constrained, which presents the challenge of obtaining detailed trajectory information subject to memory, processing, energy and storage constraints.

Consider tracking of flying foxes as a motivating scenario. The computing platform is inaccessible once deployed and it is constrained in computational resources. The position data, on the other hand, is acquired in a stream fashion. The RAM

available on the platform barely reaches 4 KBytes, while the storage space is only 1 MB to store trajectories over weeks and months before they can be offloaded. The combination of long-term operational requirement and constrained resources therefore requires an intelligent online algorithm that can process the incoming points instantaneously, i.e in constant space and time, and that can achieve high compression rate.

Current trajectory compression algorithms often fail to operate under such requirements, as they either require substantial amount of buffer space or require the entire data stream [6][7]. Existing online algorithms operate retrospectively on trajectory data or assume favourable trajectory characteristics, resulting in the worst-case complexity of their online performance ranging from $\mathcal{O}(n \log n)$ to $\mathcal{O}(n^2)$ [8]. The high complexity of existing methods limits their utility in resource-constrained environments. To address this challenge, we propose the Bounded Quadrant System (BQS), an online algorithm that can run sustainably on resource-constrained devices. Its fast version achieves $\mathcal{O}(n)$ time and $\mathcal{O}(1)$ space complexity while providing guaranteed error bounds. By using a convex hull that is formed by a bounding box and two angular bounds around all points, the algorithm is able to make quick compression decisions without iterating through the buffer and calculating the maximum error in most of the cases. Using empirical GPS traces from the flying fox scenario and from cars, we evaluate the performance of our algorithms and quantify their benefits in improving the efficiency of trajectory compression.

In summary, our contributions are three-fold:

- Proposal of an efficient online trajectory compression algorithm. The algorithm uses convex hull bounding to compress incoming points into trajectory segments with error guarantees. The fast version of the algorithm achieves constant time and space complexity for each step, or equivalently $\mathcal{O}(n)$ time complexity and $\mathcal{O}(1)$ space complexity for the whole data stream.
- Demonstration of the generality and extensibility of the proposed algorithm to support the 3-D case and a different error metric.
- Comprehensive evaluation of the algorithm using real-life data collected from wildlife tracking and vehicle tracking applications as well as synthetic data.

The remainder of this paper is organized as follows. The

next section surveys related work. We then motivate the need for a new online trajectory compression algorithm by describing our hardware platform and the data acquisition process. The BQS algorithms are presented subsequently. A discussion on how to generalize the BQS algorithm to a higher dimension is provided. Finally, we evaluate BQS on empirical and synthetic traces, and conclude the paper.

II. RELATED WORK

The rapid increase in the number of GPS-enabled devices in recent years has led to an expansion of location-based services and applications and our increased reliance on localization technology. One challenge that location-based applications need to overcome is the amount of data that continuous location tracking can yield. Efficient storage and indexing of these datasets is critical to their success, especially for embedded and handheld devices which provide users with location context in-situ.

Several trajectory compression algorithms that offer significant improvements in terms of data storage have been proposed in the literature. We focus our review on lossy compression algorithms as they provide better trade-offs between high compression ratios and an acceptable error of the compressed trajectory.

Douglas and Peucker were amongst the first to propose an algorithm for reducing the number of points in a digital trajectory [6]. The Douglas-Peucker algorithm starts with the first and last points of the trajectory and repeatedly adds intermediate points to the compressed trajectory until the maximum spatial error of any point falls below a predefined threshold. The algorithm guarantees that the error of the compressed trajectory is within the bounds of the target application, but due to its greedy nature, it achieves relatively low compression ratios. The worst-case runtime of the algorithm is $\mathcal{O}(n^2)$ with n being the number of points in the original trajectory which has been improved by Hershberger et al to $\mathcal{O}(n \log n)$ [7].

The disadvantage of the Douglas-Peucker algorithm is that it runs off-line and requires the whole trajectory. This is of limited use for modern location-aware applications that require online processing of location data. A generic sliding-window algorithm (conceptually similar to the one summarized in [9]) is often used to overcome this limitation and works by compressing the original trajectory over a moving buffer. The sliding-window algorithm can run online, but its worst-case runtime is still $\mathcal{O}(nL)$ where L is the maximum buffer size. On the other hand, multiple examples of fast algorithms exist in the literature [10][11]. These algorithms, however, do not apply to our scenario as they only run off-line and cannot support location-aware applications in-situ.

SQUISH [12] has achieved relatively low runtime, high compression ratios and small trajectory errors. However, its disadvantage was that it could not guarantee trajectory errors to be within an application-specific bound. A follow up work presented SQUISH-E [8] that provides options to both minimize trajectory error given a compression ratio and to maximize compression ratio given an error bound. The worst-case runtime of SQUISH-E algorithms is $\mathcal{O}(n \log \frac{n}{\lambda})$, where λ

is the desired compression ratio. While the compression ratio-bound flavor of SQUISH-E can run online, the error-bound version runs offline only.

The disadvantage of these algorithms that repeatedly iterate through all points in the original trajectory is their long runtime. SQUISH-E is approaching linear computational complexity for large compression ratios, however, the resulting compressed trajectory has unbounded error. Our motivation is to develop algorithms that can fit the computational and space constraints of energy-constrained devices and that can be used to track locations of small objects or animals over long time periods with bounded errors. More complex algorithms, such as STTrace [13] that uses estimation of speed and heading to predict the position of the next location or the MBR algorithm [14] that maintains, divides, and merges bounding rectangle representing the original trajectory fall outside of capabilities of our target hardware platform, which is described in detail in the following section.

In contrast to existing methods, our approach achieves constant time and space complexity for each point by only considering the most recent minimal bounding convex-hulls. We show in the evaluation section that the compression ratios that our approach achieves are superior to those of the related trajectory compression algorithms. Although simplistic approaches such as Dead Reckoning [15][16] achieve comparable runtime performance, we show that our algorithm significantly outperforms these protocols in compression ratio while guaranteeing an error bound.

III. BACKGROUND

In this section, we present the background of the study. The hardware system architecture used in the real-life bat tracking application is described. We also briefly introduce two existing solutions [17][9], for two reasons. First, by analyzing the existing algorithms we provide insights about why we need a better algorithm. Second, these two algorithms will be evaluated along with the proposed algorithm in a comparative study in the experiments.

A. Motivating Scenario

We employ the Camazotz mobile sensing platform [4], which has been specifically designed to meet the stringent constraints for weight and size when being employed for wildlife tracking, in particular for different species of flying foxes, also known as megabats (Pteropus). Animal ethics requires that the total payload weight is smaller than a certain percentage (usually below 5%) of the animal's body weight, which corresponds to a weight limit of roughly 20-30 g for flying foxes. Camazotz is a light-weight but feature-rich platform built around the Texas Instrument CC430F5137 system on chip, which integrates a 16-bit microcontroller (32 KBytes ROM, 4 KBytes RAM) and a short-range radio in the 900 MHz frequency band. We use a rechargeable Lithium-ion battery connected to a solar panel to provide power to the device. Several on-board sensors such as temperature/pressure sensor, accelerometer/magnetometer and a microphone allow for multi-modal activity detection [4] and sensing of the animal's

environment. A ublox MAX6 receiver allows to determine the current position using the Global Positioning System (GPS). Sensor readings and tracking data can be stored locally in external flash storage (1 MByte) until the data can be uploaded to a base station deployed at animal congregation areas using the short range radio transceiver. We also employ the same hardware placed on the dashboard of a car to capture mobility traces of vehicles in urban road networks.

The GPS traces collected by such platforms are often used to model and analyze the mobility and the behavior of the moving object. Hence, it is most important to gather information for the object's major movements. The areas where it often visits, the route it takes to travel between its places of interests, and the time windows in which it usually makes the travels, are the key features we want to extract from the traces. However, the hardware limitations of the platform constrain its capability to capture such information in the long term. Motivated by this application, we propose to use online trajectory compression on such resource-constrained platforms to reduce the data size. The compression will introduce a bounded error and discard some information for small movements, but will capture the interesting moments when major traveling occurs.

B. Existing Solutions

1) *Buffered Douglas-Peucker*: Douglas-Peucker (DP) [17] is a well-known algorithm for trajectory compression. In our scenario, in which the buffer size is largely constrained due to memory space limit on the platform, we are still able to apply DP on a smaller buffer of data. We call this algorithm Buffered Douglas-Peucker (BDP). That is, the incoming points are accumulated in the buffer until it is full, then the partial trajectory defined by the buffered points is processed by the DP algorithm. However, such solution has inferior compression rates mainly due the extra points taken when the buffer is repeatedly full, preventing a desirable high compression rate from being achieved.

A result of using DP with a fixed-size buffer is that both the first and last points in the buffer are kept in the compressed output every time the buffer is full, even when they can actually be discarded safely. In the worst case scenario where the object is moving in a straight line from the start to the end, this solution will use $\lceil \frac{N}{M} \rceil + 1$ points, where N is the number of total points and M is the buffer size. In contrast, the optimal solution needs to keep only two points. Although the overhead depends on the shape of the trajectory and the buffer size, generally BDP takes considerably more points than necessary, particularly for small buffer sizes.

2) *Buffered Greedy Deviation*: Buffered Greedy Deviation (BGD, a variation of the generic sliding-window algorithm) represents another simplistic approach. In this strategy whenever a point arrives, we append the point to the end of the buffer, and do a complete calculation of the error for the trajectory segment defined by the points in the buffer to the line defined by the start point and the end point. If the deviation already exceeds the tolerance, then we keep the last point in the compressed trajectory, clear the buffer and start a new segment at the last point. Otherwise the process continues for the next incoming point.

The algorithm is easy to implement and guarantees the error tolerance, however it too has a major weakness. The compression rate is heavily dependent on the buffer size, as it faces the same problem as BDP. If we increase the buffer size, because the time complexity is $\mathcal{O}(n^2)$, the computational complexity would increase drastically, which is undesirable in our scenario because of the energy limitations. Therefore, BGD represents a significant compromise on the performance as it has to make a direct trade-off between time complexity and compression rate.

Clearly, a more sophisticated algorithm that can guarantee the bounded error, process the point with low time-space complexity, and achieve high compression rate is desired. We propose an algorithm called Bounded Quadrant System (BQS) to address this problem. Before delving into the details, we present some notations, definitions and theorems to help the reader understand BQS's working mechanism.

IV. PRELIMINARIES

In this section we provide a series of definitions and theorems as the necessary foundations for further discussion.

Location Point A location point $v = \langle \text{latitude}, \text{longitude}, \text{timestamp} \rangle$ is a tuple that records the spatio-temporal information of a location sample.

Segment and Trajectory A trajectory segment is a set of location points that are taken consecutively in the temporal domain, denoted as $\tau = \{v_1, \dots, v_n\}$. A trajectory is a set of consecutive segments, denoted as $\mathbb{T} = \{\tau_1, \tau_2, \dots\}$.

Given the definitions of segment and trajectory, we introduce the concept of compressed trajectory with bounded error:

Deviation Given a trajectory segment $\tau = \{v_1, \dots, v_n\}$, the deviation $d(\tau)$ is defined as the largest distance from any location $v_i \in \{v_2, \dots, v_{n-1}\}$ to the line defined by v_1 and v_n . The trajectory deviation is defined as the maximal segment deviation from any of its segments, as $\max(d(\tau_i)), \tau_i \in \mathbb{T}$.

Deviation is a distance metric to measure the maximum error from the compressed trajectory segment to the original segment. For simplicity of the proof and presentation, without loss of generality, we use point-to-line distance in this definition. Note that point-to-line-segment distance can be easily used within BQS too.

Key Point Given a trajectory segment buffer $\tau = \{v_1, \dots, v_k\}$ and a deviation threshold ϵ^d , a new location point v_n, v_k is a key point if $d(\tau) \leq \epsilon^d$ and $d(\tau \cup \{v_n\}) > \epsilon^d$, where ϵ^d is the error tolerance.

In other words, when a new point is sampled, the immediate previous point is classified as a key point if the new point results in the maximum error of any point in the segment buffer exceeding ϵ^d .

Compressed Trajectory Given a trajectory segment $\tau = \{v_1, \dots, v_n\}$, its compressed trajectory segment is defined by the start and end location v_1 and v_n , and is denoted as $\tau' = \{v_1, v_n\}$. The compressed trajectory $\mathbb{T}' = \{v_i, v_j, \dots, v_k\}$

of \mathbb{T} is the set of starting and ending locations of all the segments in \mathbb{T} , ordered by the position of its source segment in the original trajectory.

Error-bounded Trajectory An error-bounded trajectory is a compressed trajectory with the deviation for any of its compressed segments smaller than or equal to a given error tolerance ϵ^d . Formally: given a trajectory $\mathbb{T} = \{\tau_1, \dots, \tau_k\}$, and its compressed trajectory $\mathbb{T}' = \{v_i, v_j, \dots, v_k\}$, \mathbb{T}' is error-bounded by ϵ^d if $\forall \tau'_i \in \mathbb{T}', d(\tau'_i) \leq \epsilon^d$.

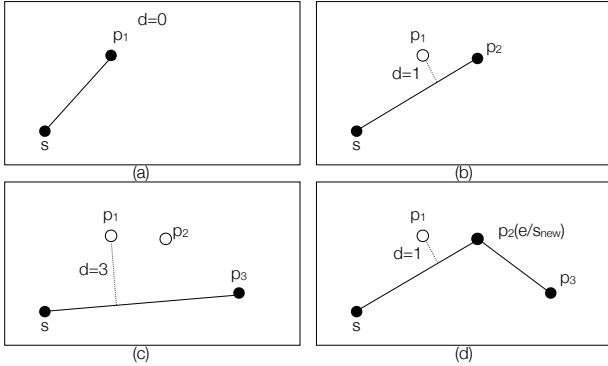


Fig. 1: Error-bounded Compression ($\epsilon = 2$)

Figure 1 demonstrates the process of error-bounded trajectory compression. Assuming that the current trajectory segment starts from s , when adding the first point p_1 (Figure 1(a)), the deviation is 0. Hence we proceed to the next incoming point p_2 (Figure 1(b)). Here the deviation is 1, which lies within the error tolerance, so the current segment can be safely represented by $\overline{sp_2}$. However after p_3 arrives, the deviation of the segment reaches $3 > \epsilon$ because of p_1 (Figure 1(c)). Clearly p_3 should not be included in the current trajectory segment. Instead, the current segment ends at p_2 and a new segment is then started at p_2 (Figure 1(d)). The new segment includes p_3 and repeats the above process for new incoming points until the error tolerance is exceeded again. Such process guarantees that any trajectory segment has a smaller deviation than ϵ .

When a trajectory is turned into a compressed trajectory, the temporal information it carries changes representation too. Instead of having a timestamp at every location point in the original trajectory, the compressed trajectory uses the timestamps of the key points as the anchors to reconstruct the time sequences. Given a trajectory segment defined by two key points v_s, v_e , the reconstructed location at timestamp \bar{t} ($v_s.t \leq \bar{t} \leq v_e.t$) is defined as:

$$v_{\bar{t}} = \langle h_{lat}(P, v_s, v_e, \bar{t}), h_{lon}(P, v_s, v_e, \bar{t}), \bar{t} \rangle. \quad (1)$$

where function h is an interpolation function that uses a distribution function P , a start value, an end value, and a timestamp at which the value should be interpolated. P interpolates the location at a timestamp according to a distribution. As an example, the h and P functions for interpolating the latitude can be defined as:

$$P(\bar{t}) = \frac{\bar{t} - v_s.t}{v_e.t - v_s.t} \quad (2)$$

$$h_{lat}(P, v_s, v_e, \bar{t}) = v_s.lat + P(\bar{t}) \times (v_e.lat - v_s.lat) \quad (3)$$

where P is set to reconstruct the uniform distribution. However, in practice this function can be derived online to fit the distribution of the actual data. For instance, an online algorithm for fitting Gaussian distribution by dynamically updating the variance and mean can be implemented with semi-numeric algorithms described in [18], which can be used to derive P .

As we are designing an online algorithm where each point is processed only once, the problem is turned into answering the following question: does the incoming point result in a new compressed trajectory segment or can it be represented in the previous compressed trajectory segment? To address this question, we first provide an overview and then the details for the BQS framework.

V. TRAJECTORY COMPRESSION WITH BOUNDED QUADRANT SYSTEM

A. Overview

The motivation of the algorithm is that we need a trajectory management infrastructure to store historical trajectory data with minimal storage space while maintaining the error-bounds and capturing the major movements of the mobile object. Hence we need an efficient online trajectory compression algorithm, that yields error-bounded results in low time and space complexity and that minimizes the number of points taken, i.e. the Bounded Quadrant System (BQS).

A BQS is a convex hull that bounds a set of points (an example is shown in Figure 2). A BQS is constructed by the following steps:

- 1) For a trajectory segment, we split the space into four quadrants, with the origin set at the start point of the current segment, and the axes set to the UTM(Universal Transverse Mercator) projected x and y axes.
- 2) For each quadrant, a bounding box is set for the buffered points in that quadrant, if there are any. There can be at most four BQS for a trajectory segment.
- 3) We keep two bounding lines that record the smallest and greatest angles between the x axis and the line from the origin to any buffered point for each quadrant.
- 4) We have at most eight significant points in every quadrant systems - four vertices on the bounding box, four intersection points from the bounding lines intersecting with the bounding box. Some of the points may overlap.
- 5) Based on the deviations from the significant points to the current path line, we have a group of lower bound candidates and upper bound candidates for the maximum deviation. From these candidates we derive a pair of lower bound and upper bound $\langle d^{lb}, d^{ub} \rangle$, to make compression decisions without the full computation of segment deviation in most of the cases.

Here the lower bound d^{lb} represents the smallest deviation possible for all the points in the segment buffer to the start point, while the upper bound d^{ub} represents the largest deviation possible for all the points in the segment buffer to the start point. With d^{lb} and d^{ub} , we have three cases:

- 1) If $d^{lb} > \epsilon^d$, it is unnecessary to perform deviation calculation because the deviation is guaranteed to break the tolerance, so a new segment needs to be started.

- 2) If $d^{ub} \leq \epsilon^d$, it is unnecessary to perform deviation calculation because the deviation is guaranteed to be smaller or equal to the tolerance, so the current point will be included in the current segment, i.e. no need to start a new segment.
- 3) If $d^{lb} \leq \epsilon^d < d^{ub}$, a deviation calculation is required to determine whether the actual deviation is breaking the tolerance.

Hence a pair of bounds is considered “tight” if the difference between them is small enough that it leaves minimum room for the error tolerance ϵ^d to be in between them.

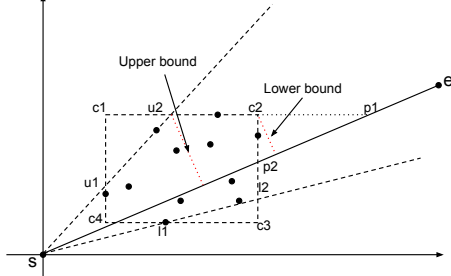


Fig. 2: An Example of the BQS

B. The Bounded Quadrant System

An illustration of a BQS is provided in Figure 2. Here we have a BQS in the first quadrant. Note that it shows only one BQS but in reality there could be at most four BQS for each segment, one for each quadrant. In the figure, s is the start point of the current segment, which is also used as the origin of the BQS. The solid black dots are the buffered points for the current segment. The bounding box $\overline{c_1c_2c_3c_4c_1}$ is the minimum bounding rectangle for all the points in the first quadrant. The bounding lines $\overline{su_2}$ and $\overline{sl_2}$ record the greatest and smallest angles that any line from the origin to the points can have (w.r.t. the x axis), respectively.

The intuition of the BQS structure is to exploit the favorable properties of the convex hull formed by the significant points from the bounding box and bounding lines for the buffered points (excluding the start point). That is, with the polygons formed by the bounding box and the bounding lines, we can derive a pair of tight lower bound and upper bound on the deviation from the points in the buffer to the line defined by the start and end points denoted as $l_{s,e}$. With such bounds, most of the deviation calculations on the buffered points are avoided. Instead we can determine the compression decisions by only assessing a few significant vertices on the bounding polygon. The splitting of the space into four quadrants is necessary as it guarantees a few useful properties to form the error bounds. More details are provided in Section VIII.

To understand how the BQS works, we use the example with a start point s , a few points in the buffer, and the last incoming point e as in Figure 2. The goal is to determine whether the deviation will be greater than the threshold if we include the last point in the current segment. First we present two fundamental theorems:

Theorem 5.1: Assume that a point p satisfies $d(p, s) \leq \epsilon$, where s is the start point, then

$$d^{max}(p, l_{s,e}) \leq \epsilon \quad (4)$$

regardless of the location of the end point e .

Proof: Trivial. This theorem enables the quick decision on an incoming point even without assessing the bounding boxes or lines. Such a point is directly “included” in the current segment, and the BQS structure will not be affected.

Theorem 5.2: Assume that the buffered points $\{p_i\}$ are bounded by a rectangle in the spatial domain, with the vertices c_1, c_2, c_3, c_4 , if we denote the line defined by the start point s and the end point e as $l_{s,e}$, then we always have:

$$d^{max}(p_i, l_{s,e}) \geq \min\{d(c_i, l_{s,e})\} = d^{lb} \quad (5)$$

$$d^{max}(p_i, l_{s,e}) \leq \max\{d(c_i, l_{s,e})\} = d^{ub} \quad (6)$$

Proof: The proof of this theorem is fairly straightforward if we regard the polygon $\overline{c_1c_2c_3c_4c_1}$ as a convex hull. Nevertheless we give an alternative proof in details to help readers understand the concept. The bounding box dictates that on each of its edges there must be at least one point. If for any edge $\overline{c_jc_k}$ of the bounding box we denote a buffered point on it as p^e , then we have $\min\{d(c_j, l_{s,e}), d(c_k, l_{s,e})\} \leq d(p^e, l_{s,e}) \leq \max\{d(c_j, l_{s,e}), d(c_k, l_{s,e})\}$. Consolidating the bounds on all of the edges, we have the proof of the theorem.

Theorems 5.1 and 5.2 show how some of the points can be safely discarded and how the basic lower bound and upper bound properties are derived. However, Theorem 5.2 only provides a pair of loose bounds that can hardly avoid any deviation computation. To obtain tighter and useful bounds, we need to introduce a few advanced theorems. Throughout the theorem definitions we use the following notations:

- **Corner Distances:** We use $d^{corner} = \{d(c_i, l_{s,e})\}$, $i \in \{1, 2, 3, 4\}$ to denote the distances from each vertex of the bounding box to the current path line.
- **Near-far Corner Distances:** We use $d^{corner-nf} = \{d(c_n, l_{s,e}), d(c_f, l_{s,e})\}$, to denote the distances from the nearest vertex c_n and the farthest vertex c_f of the bounding box (near and far in terms of the distance to the origin) to the current path line. The nearest and farthest corner points are determined by the quadrant the BQS is in. For example, in Figure 2 $c_n = c_4$ and $c_f = c_2$.
- **Intersection Distances:** We use $d^{intersection} = \{d(p, l_{s,e})\}$, $p \in \{l_1, l_2, u_1, u_2\}$ to denote the distances from each intersection point to the current path line, where l_i are the intersection points of the lower angle bounding line and the bounding box, and u_i are the intersection points of the upper angle bounding line and the bounding box.

Some advanced bounds are defined as follows:

Theorem 5.3: Given a BQS, if the line $l_{s,e}$ is in the quadrant, and $l_{s,e}$ is in between the two bounding lines ($\theta_{lb} \leq \theta_{s,e} \leq \theta_{ub}$), then we have the following bounds on the segment deviation:

$$d^{max}(p, l_{s,e}) \geq d^{lb} = \quad (7)$$

$$\max \begin{cases} \min\{l_1, l_{s,e}\}, d(l_2, l_{s,e}) \\ \min\{d(u_1, l_{s,e}), d(u_2, l_{s,e})\} \\ \max\{d^{corner-nf}\} \end{cases}$$

$$d^{max}(p, l_{s,e}) \leq d^{ub} = \max\{d^{intersection}\} \quad (8)$$

A line l is “in” the quadrant Q if the angle θ^l between l and the x axis satisfies $\theta_{start}^Q \leq \theta^l < \theta_{end}^Q$ or $\theta_{start}^Q \leq \theta^l + \pi < \theta_{end}^Q$ or $\theta_{start}^Q \leq \theta^l - \pi < \theta_{end}^Q$, where θ_{start}^Q and θ_{end}^Q are the angle range of the quadrant where the BQS resides. Note that this definition is distance metric-specific. Since we use point-to-line distance, a line is automatically “in” exactly two quadrants. In future references we assume θ^l satisfies $\theta_{start}^Q \leq \theta^l < \theta_{end}^Q$ if it is “in” the quadrant.

Theorem 5.4: Given a BQS, if the line $l_{s,e}$ is in the quadrant, and $l_{s,e}$ is outside the two bounding lines ($\theta_{ub} < \theta_{s,e}$ or $\theta_{lb} > \theta_{s,e}$), we have the same bounds on the segment deviation as in Theorem 5.3.

If the path line is not in the same quadrant with the BQS, we use Theorem 5.5 to derive the bounds:

Theorem 5.5: Given a BQS, if the line $l_{s,e}$ is not in the quadrant, the bounds of the segment deviation are defined as:

$$d^{max}(p, l_{s,e}) \geq d^{lb} = \quad (9)$$

$$max \begin{cases} \min\{d(l_1, l_{s,e}), d(l_2, l_{s,e})\} \\ \min\{d(u_1, l_{s,e}), d(l_2, l_{s,e})\} \\ 3^{rd} - largest\{d^{corner}\} \end{cases}$$

$$d(p, l_{s,e}) \leq max\{d^{corner}\} = d^{ub} \quad (10)$$

Proof of the theorems is provided in the appendix.

C. The BQS Algorithm

The BQS algorithm is formally described in Algorithm 1:

Algorithm 1: The BQS Algorithm

Input: Start point s , incoming new point e , buffered points \mathcal{B} , deviation threshold ϵ^d

Algorithm:

- 1: **if** $d(s, e) \leq \epsilon^d$ **then**
- 2: *Decision:* $e \rightarrow \mathcal{B}$
- 3: **else**
- 4: Assume e is the end point, compute the lower bound d_i^{lb} and upper bound d_i^{ub} of the maximal deviations for the points in each quadrant using Theorems 5.3, 5.4, 5.5
- 5: Aggregate all the lower bounds and upper bounds in each BQS by computing. $d^{lb} = max\{d_i^{lb}\}$ and $d^{ub} = max\{d_i^{ub}\}$
- 6: **if** $d^{ub} \leq \epsilon^d$ **then**
- 7: *Decision:* $e \rightarrow \mathcal{B}$
- 8: **else if** $d^{lb} > \epsilon^d$ **then**
- 9: *Decision:* Current segment stops and new segment starts at the previous point before e
- 10: **else if** $d^{lb} \leq \epsilon^d < d^{ub}$ **then**
- 11: $d = ComputeDeviation(\mathcal{B}, l_{s,p})$
- 12: *Decision:* made according to d
- 13: **end if**
- 14: **end if**
- 15: Determine which quadrant e lies in and update the bounding structure for the corresponding BQS

The algorithm starts by checking if there is a trivial decision: by Theorem 5.1, if the incoming point e lays within the range of ϵ of the start point, no matter where the final end point is, the point will not result in a greater deviation than ϵ (Lines 1-3). After e passes this test, it means e may result in a greater deviation from the buffered points. So we assume that e is the new end point, and assume the current segment is presented by $l_{s,e}$. Now for each quadrant we have a BQS, maintaining their respective bounding boxes and bounding lines. For each BQS, we have a few (8 at most) significant points, identified as the four corner points of the bounding box and the four intersection points between the bounding lines and the bounding box. According to the theorems we defined, we can aggregate four sets of lower bounds and upper bounds for each quadrant, and then a global lower bound and a global upper bound for all the quadrants (Lines 4-5). According to the global lower bound and upper bound, we can quickly make a compression decision. If the upper bound is smaller than ϵ , it means no buffered point will have a deviation greater than or equal to ϵ , so the current point e is immediately included to the current trajectory segment and the current segment goes on (Lines 6-7). On the contrary, if the lower bound is greater than ϵ , we are guaranteed that at least one buffered point will break the error tolerance, so we save the current segment (without e) and start a new segment at e (Lines 8-9). Otherwise if the tolerance happens to be in between the lower bound and the upper bound, an actual deviation computation is required, and decision will be made according to the result (Lines 10-13). Finally, if the current segment goes on, we put e into its corresponding quadrant and update the BQS structure in that quadrant (Line 14).

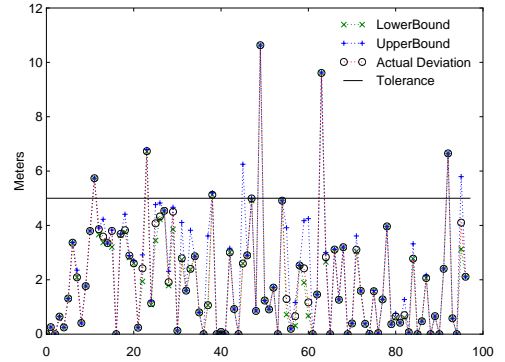


Fig. 3: Bounds v.s. Actual Deviation

Figure 3 demonstrates the lower and upper bounds of some randomly-chosen location points from the real-life flying fox dataset, with ϵ^d set to 5 m. The x axis shows the indices of the points, while the solid horizontal line indicates the error tolerance. It is evident that in most cases the bounds are very tight and that in more than 90% of the occasions we can determine if a point is a key point by using only the bounds and avoid actual deviation calculations.

D. Data-centric Rotation

A technique called data-centric rotation is used to further tighten the bounds. When a new segment is started, instead

of constructing and updating the BQS immediately after the arrival of new points, we allow a tiny buffer to store the first few points (e.g. 5) that are not in the range of ϵ within the start point (meaning that these points will actually affect the bounding box). With the buffer, we compute the centroid of the buffered points, and rotate the current x axis to the line from the start point to the centroid. By applying this rotation, we enforce that the points are split into two BQS. This improves the tightness of the bounds because the bounding convex-hulls are generally tighter with less spread. Once the rotation angle is identified, each new point for the same segment is temporally rotated by the same angle when estimating their distances to the line $l_{s,e}$.

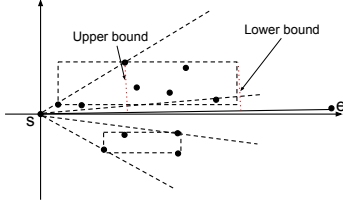


Fig. 4: Data-centric Rotation

Figure 4 shows the effect of this rotation. The points are the same as in Figure 2, but in this figure they are rotated to “center” the data points to the x axis. After the rotation the points are split into two BQS and it’s visually evident that the gap between the lower bound and the upper bound becomes smaller. As in reality the likelihood is substantial for a moving object to travel in a major direction despite slight heading changes, this step improves the BQS’s pruning power significantly. The procedure is applied on Algorithm 1.

E. Achieving Constant Time and Space Complexity

With the pruning power introduced by the deviation bounds, Algorithm 1 achieves excellent performance in terms of time complexity. Its expected time complexity is $\alpha \times n \times c_1 + (1 - \alpha) \times n \times m \times c_2$, where α is the pruning power, m is the maximum buffer size, and c_1, c_2 are two constants denoting the cost of the processing of each point. Empirical study in the next section shows that α is generally greater than 0.9, meaning the time complexity is approaching $\mathcal{O}(n)$ for the whole data stream. However, the theoretical worst case time complexity is still $\mathcal{O}(n^2)$. Moreover, because we keep a buffer for the points in the current segment for potential deviation calculation, the worst-case space complexity is $\mathcal{O}(n)$. To further reduce the complexity, we propose a more efficient algorithm that still utilizes the bounds but is able to completely avoid any full deviation calculation and any use of buffer, making the time and space costs of processing a point constant.

The algorithm is nearly identical to Algorithm 1. The major difference is that whenever the case $d^{lb} \leq \epsilon^d < d^{ub}$ occurs (Line 10), an aggressive approach is taken. No deviation calculation is performed, instead we take the point and start a new trajectory segment to avoid any computation and to eliminate the necessity of maintaining a buffer for the points in the current segment. So Lines 11-12 in Algorithm 1 are changed into making the “stop and restart” decision (as in

Line 9) directly without any full calculation in Line 12. Also, the maintenance of the buffer is not needed any more.

The Fast BQS (FBQS) algorithm takes slightly more points than Algorithm 1 in the compression, reducing the compression rate by a small margin. However, the simplification on the time and space complexity is significant. The fast BQS algorithm achieves constant complexity in both time and space for processing a point. Equivalently, time and space complexity are $\mathcal{O}(n)$ and $\mathcal{O}(1)$ for the whole data stream.

The time complexity is only introduced by assessing and updating a few key variables, i.e. bounding lines, intersection points and corner points. We can now arrive at the compression decision by keeping only the significant BQS points of the number $c \leq 32$ (4 corner points and 4 intersection points at most for each quadrant) for the entire algorithm.

When the buffer size is unconstrained, the three algorithms Buffered Douglas-Peucker (BDP), Buffered Greedy Deviation (BGD) and Fast BQS (FBQS) have the following worst-case time and space complexity:

TABLE I: Worst-case Complexity

	Time	Space
FBQS	$\mathcal{O}(n)$	$\mathcal{O}(1)$
BDP	$\mathcal{O}(n^2)$	$\mathcal{O}(n)$
BGD	$\mathcal{O}(n^2)$	$\mathcal{O}(n)$

F. Maintenance Procedures

In addition to the compression itself, the BQS framework employs two techniques to further reduce the storage space required for the historical data, namely error-bounded merging and error-bounded ageing. Due to space limitations, we only give a brief description of the techniques. More details will be incorporated in an extended version of this work.

Merging is a procedure in which the newly compressed segment is used as a query to search similar historical segments in the trajectory database. If any existing compressed segment could represent the same path with a minor error, the new segment is considered duplicate information and is merged into the existing one.

Ageing is based on the intuition that newer and older trajectories should not bear the same significance in the historical trajectory database. More recent trips represent the moving object’s recent travel patterns better and should be regarded of greater interest. Hence the ageing procedure re-runs the compression algorithm on the existing trajectories that are already compressed, but with a greater error tolerance, so that the compression rate will be further improved.

The procedures are aligned with our goal, namely capturing the spatio-temporal characteristics such as the time windows, destinations and routes for the major movements of the moving object. By making a more aggressive trade-off between accuracy and coverage, it further extends the frameworks capability to capture mobility patterns over long periods.

G. Generalization

The BQS algorithm’s advantage is not only in its competitive complexity and compression rate, but also in its extensibility to

derive other variations for different application requirements. In this section we briefly introduce a 3-D variant of the BQS algorithm to demonstrate its extensibility for more complex application requirements such as 3-D location tracking and time-sensitive tracking.

In some scenarios such as indoor tracking or aero vehicle tracking, the tracking process takes places in a 3-D geographic space [19]. At any timestamp, the moving object has not only the latitude and longitude coordinates, but also the altitude component. The simplification error is then determined by the maximum deviation from the original trajectory in this 3-D space defined by $\langle \text{latitude}, \text{longitude}, \text{altitude} \rangle$.

In some location tracking applications it is desirable to know where the moving object is at a certain time. Therefore, time-sensitive error such as in [20] becomes a useful error metric in such scenarios. Under such settings, instead of deriving the deviation from the original trajectory solely in the $\langle \text{latitude}, \text{longitude} \rangle$ plane, the error is also attributed by the time axis in a three dimensional space $\langle \text{latitude}, \text{longitude}, \text{timestamp} \rangle$.

Both applications require a trajectory compression algorithm that can handle 3-D data. Now we show that extending the BQS algorithm to the 3-D space is a straightforward process. Let us revisit the example we discussed in Figure 2, where we demonstrated the concept of bounding box and bounding line in the 2-D case. For the 3-D case, instead of using bounding boxes and bounding lines, we use bounding right rectangular prisms and bounding planes to bound the location points. An illustration is given in Figure 5.

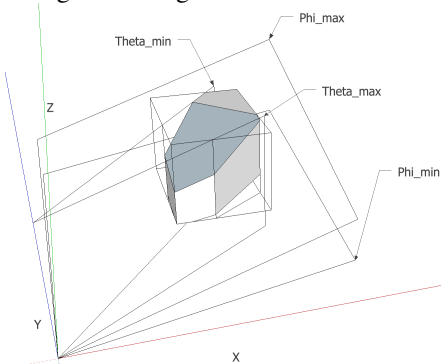


Fig. 5: The 3-D version of BQS illustrated

In Figure 5, we use a Cartesian coordinate system to represent the 3-D space. Any location point is defined by a coordinate tuple $\langle x, y, z \rangle$, where the z axis can either represent the timestamp or the altitude. The deviation metric is also extended to measure the maximum distance from original 3-D points to a 3-D line.

There are eight quadrants in total. We use the first quadrant ($x > 0 \wedge y > 0 \wedge z > 0$) as a demonstration in the figure. A bounding prism is used to bound the location points in each quadrant, as a direct extension to the 2-D case. Then, in each quadrant, we also establish two pairs of bounding planes to maintain the minimum and maximum angles to their respective reference planes. We have a pair of “vertical” bounding planes $\Theta_{min}, \Theta_{max}$, which both are orthogonal to the XY plane and

contain the z axis. They represent the minimum and maximum angles formed by any plane that contains a location points to the YZ plane. Similarly, we have the “inclined” bounding planes Φ_{min} and Φ_{max} . They represent the minimum and maximum angles between the planes in $\{\Phi_i\}$ to the XY plane. Any Φ_i is determined by three points, namely two anchor points and one data point, and all Φ_i in a quadrant share the same anchor points. The anchor points are determined by the quadrant, as $(\text{sign}(x) \times 1, -\text{sign}(y) \times 1, 0), (-\text{sign}(x) \times 1, \text{sign}(y) \times 1, 0)$. For this quadrant, the two anchor points are $(1, -1, 0)$ and $(-1, 1, 0)$.

The bounding prism is hence “cut” into a 3-D polyhedron that is also a convex hull (shadowed part in Figure 5), and the vertices that form the hull are the significant points we use to quickly derive error bounds. There are mature software libraries to enable the efficient calculation of the bounding polyhedron, such as GEOS¹ or CGAL². In practice, to further improve the efficiency of the computation of the convex hull, we only consider the intersection points between the bounding planes and the bounding prism, while intersections between bounding planes are not considered. This will slightly increase the volume of the bounding polyhedron but the computational cost will decrease considerably and become stable (independent of the spatial relations among bounding planes). Finally, we obtain a 3-D convex hull formed by at most 17 points (at most 4 intersection points for each bounding plane, plus the farthest vertex to the origin of the prism). Using similar techniques to Theorems 5.3, 5.4 and 5.5, new pruning rules for the 3-D BQS can then be derived based on the significant points. The computation involved for identifying the significant points is more complex than that in the 2-D case, but overall the algorithm still has constant time and space complexity in its fast version setup.

It is worth noting that besides the extended version in the 3-D space, the BQS algorithm can also be used with different distance metrics, such as the point-to-line-segment distance. In cases where line-to-segment distance is used, Theorems 5.3 and 5.4 can be used with minor modification by changing Equation 8 to:

$$d^{max}(p, \overline{s, e}) \leq d^{ub} = \max\{d^{intersection}, d^{corner-nf}\} \quad (11)$$

while Theorem 5.5 still holds. The definition of the “in quadrant” property is slightly changed accordingly.

VI. EXPERIMENTS

In this section we evaluate the performance of the proposed BQS compression framework.

A. Dataset

We use three datasets, namely the flying fox (bat) dataset, the vehicle dataset, and the synthetic dataset. The two real-life datasets comprise of 138,798 GPS samples, collected by 6 Camazotz nodes (five on bats and one on a vehicle). The total travel distances for the bat dataset and vehicle dataset are

¹<http://trac.osgeo.org/geos/>

²<http://www.cgal.org/>

7,206 *km* and 1,187 *km* respectively. The tracking periods lasted six months for the bat dataset and two weeks for the vehicle dataset.

Note that there are couple of differences between the two datasets. The vehicle dataset shows larger scales in terms of travel distances well as moving speed. For instance, the length of a car trip varies from a few kilometers to 1,000 *km* while a trip for flying-foxes are usually around 10 *km*. The car can travel constantly at 100 *km/h* on a highway or 60 *km/h* on common roads, while the common and maximum continuous flying speeds for a flying-fox are approximately 35 *km/h* and 50 *km/h*. In regard to these differences, the two datasets are evaluated with different ranges of error tolerance. With a much greater spatial scale of the movements, the error tolerance used for the vehicle dataset is generally greater.

The vehicle dataset also shows more consistency in the heading angles due to the physical constraints of the road networks. On the contrary, the bats's movements are unconstrained in the 3-D space, so their turns tend to be more arbitrary. We argue that by performing extensive experiments on both datasets, the robustness of our framework to the shape of data is demonstrated.

The synthetic dataset is generated by a statistical model that anchors patterns from real-life data, and it is used specifically for the comparison between Dead Reckoning [15] and Fast BQS (FBQS). This is because continuous high-frequency samples with speed readings are required to implement DR in an error-bounded setting, while such data is lacking in the real-life datasets. The model uses an event-based correlated random walk model to simulate the movement of the object. In the simulation, waiting events and moving events are executed alternately. The object stays at its previous location during a waiting event, and it moves in a randomly selected speed and turning angle for a randomly selected time. Note that the speed follows the empirical distribution of speed, the turning angle is drawn from the von Mises distribution [21], while the move time is exponentially distributed, corresponding to the Poisson process. The trajectories are bounded by a rectangular area of 10 *km* × 10 *km*, and the speed and turning angle follow approximately the distributions of the bat data. A total of 30,000 points are generated by the model.

B. Experimental Settings

The evaluation is done on a desktop computer, however the extremely low space and time complexity of the FBQS algorithms makes it plausible to implement the algorithms on the platform aforementioned in Section III (32 KBytes ROM, 4 KBytes RAM). Particularly, if we look into the FBQS algorithm, we only need tiny memory space to store at most 32 points besides the program image itself (4 corner points and 4 intersection points for each quadrant).

Two performance indicators, namely compression rate and pruning power are tested on the real-life datasets. We define compression rate as $\frac{N^{compressed}}{N^{original}}$ where $N^{compressed}$ is the number of points after compression, and $N^{original}$ is the number of points in the original trajectory. Pruning power is defined as $1 - \frac{N^{computed}}{N^{total}}$, where $N^{computed}$ and N^{total} are the

number of full deviation calculations and the number of total points respectively.

For compression rate, we perform comprehensive comparative study to show BQS's superiority over the other three methods, namely Buffered-DouglasPeucker (BDP), Buffered-Greedy (BGD) and Douglas Peucker (DP). DR is compared against FBQS on the synthetic dataset. For buffer-dependent algorithms, we set the buffer size to be 32 data points, the same as the memory space needed by the FBQS algorithm to hold the significant points.

To intuitively demonstrate the advantage of FBQS in compression rate, we then provide performance comparison showing the number of points taken by the FBQS algorithm and the DR algorithm on the synthetic dataset. We also show the estimated operational time of tracking devices based on such compression rate. Finally, we study comparatively the actual run time efficiency of FBQS.

For all datasets, we combine all the data points into a single data stream and use it to feed the algorithms. Then we calculate the pruning power, compression rate and number of points used.

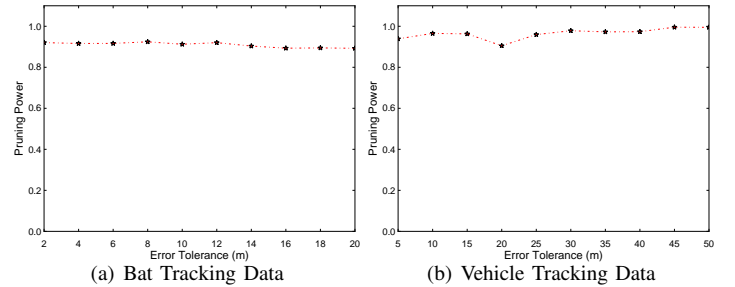


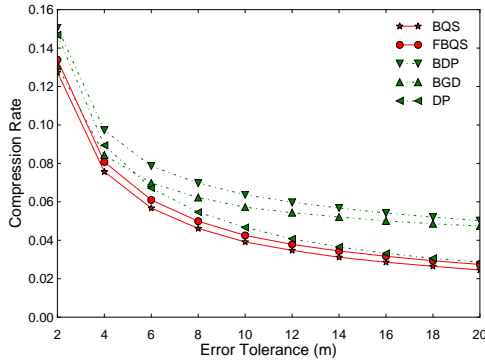
Fig. 6: Pruning Power of the BQS Algorithm (The higher the better)

C. Compression Algorithm

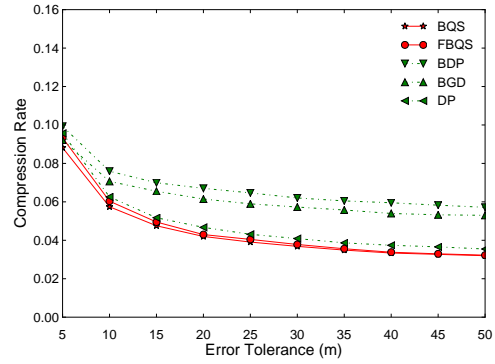
1) *Pruning Power*: Pruning power determines how efficient BQS and FBQS are. In FBQS, if the relation between the bounds and the deviation tolerance is deterministic, FBQS generates a lossless result as BQS. If it is uncertain, then FBQS will take a point regardless of the actual deviation. The pruning power reflects how often the relation is deterministic, and it indicates how many extra points could be taken by the approximate algorithm. With high pruning power, the overhead of FBQS will be small. Here we investigate the pruning power of BQS in this subsection.

Figures 6(a) and 6(b) show the pruning power achieved by BQS on both datasets. The sensitivity of the algorithm to the error tolerance or to the shape of the trajectories appears low, as the pruning power generally stays above 90% for most of the tolerance values on both datasets. This means approximately only 10% more points will be taken in the Fast BQS algorithm compared to the original BQS algorithm. The running values in Figure 3 also support this observation.

Generally, BQS shows higher pruning power on the car dataset than on the bat dataset. The higher pruning power on the vehicle data is a result of the physical constraints of the road networks, preventing abrupt turning and deviations, and making the trajectories smooth. Naturally the pruning power



(a) Bat Tracking Data



(b) Vehicle Tracking Data

Fig. 7: Comparison of Compression Rate on Real-life Datasets (The lower the better)

will be higher as a result of the higher regularity in the data's spatio-temporal characteristics.

2) *Compression Rate on Real-life Data:* Compression rate is a key performance indicator for trajectory compression algorithms. Here we conduct tests on the two real-life datasets. We compare the performance of five algorithms, namely BQS, FBQS, BDP, BGD and DP. All of the algorithms give error-bounded results. The former four are online algorithms, and the last one is offline. The compression rates are illustrated in Figures 7(a) and 7(b).

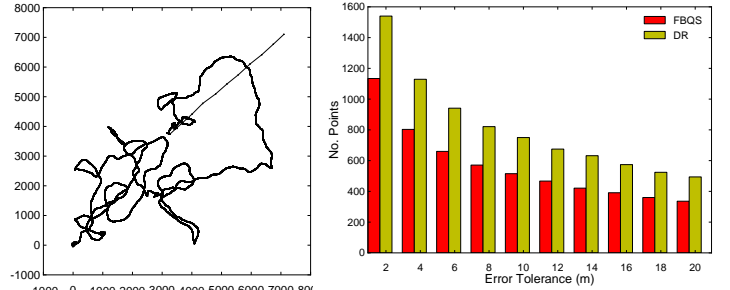
Evidently, BQS achieves the highest compression rate among the five algorithms, while BDP and BGD constantly use approximately 30% to 50% more points than BQS does. FBQS's compression rates swing between BQS's and DP's, showing the second best overall performance. BDP has the worst performance overall as it inherits the weaknesses from both DP and window-based approaches. BGD's performance is generally in between DP and BDP, but it still suffers from the excessive points taken when the buffer is full.

Comparing the two figures, it is worth noting that all the algorithms perform generally better on the bat data. Take the results at 10 m error tolerance from both figures for example, on the bat data the best and worst compression rates reach 3.9% and 6.3% respectively, while on the vehicle data the corresponding figures are 5.4% and 7.7%. This may seem to contradict the results of the pruning power. However, it is in fact reasonable because bats perform stays as well as small movement around certain locations, making those points easily discardable. Hence the room for compression is larger for the bat tracking data given the same error tolerance.

On the bat data, with 10 m error tolerance, BQS and FBQS achieve compression rates of 3.9% and 4.1% respectively. DP, as an offline algorithm that runs in $\mathcal{O}(n \log n)$ time, yields a worse compression rate than FBQS at 4.6%. Despite having poorer worst-case complexities, BDP and BGD also obtain worse compression rates than BQS and FBQS do at 6.3% and 5.8% respectively. At this tolerance, the offline DP algorithm uses approximately 20% and 10% more points than the online BQS and FBQS do, respectively. Furthermore, for online algorithms with 20 m tolerance, FBQS (2.7%) improves BDP (5.1%) and BGD (4.9%) by 47% and 45% respectively.

The results on the vehicle data show very similar trends of the algorithms' compression rate curves. Interestingly, with this dataset, because the pruning power is in most of the

cases around and above 0.95 as demonstrated in 6(b), the compression rate of FBQS is remarkably close to BQS'. For instance, at 20 m, 30 m and upwards, the difference between the two is smaller than 1%. This observation supports our aforementioned argument that the bounds of the original BQS are so effective that the number of extra points taken by FBQS is insignificant.



(a) Synthetic Dataset (unit:m)

(b) No. Points Used on Synthetic Data

Fig. 8: Shape of Synthetic Data and Comparison of Number of Points Used (The lower the better)

3) *Comparison with Dead Reckoning on Synthetic Data:* In Figure 8(a) we show the simulated trajectories from our statistical model. Visibly the trajectories show little physical constraint and considerable variety in heading and turning angles. On this dataset we study the performance comparison because on this dataset we are able to simulate the tracking node closely with high frequency sampling. Hence FBQS is used as a light-weight setup to fit such online environment.

We show in Figure 8(b) the numbers of points taken after the compression of 30,000 points under different error tolerances. With smaller ϵ such as 2 m, DR uses 1,550 points compared to 1,100 for FBQS, indicating that DR needs 40% more points. As ϵ grows, DR's performance tends to slowly approach FBQS in absolute numbers yet the difference ratio becomes more significant. At 20 m error tolerance, FBQS only takes 330 points while DR uses 500 points, the difference ratio to FBQS is around 50%.

Evidently, FBQS has achieved excellent compression rate compared to other existing online algorithms.

4) *Effect on Operational Time of Tracking Device:* Next we investigate how different online algorithms affect the maximum operational time of the targeted device. This operational time indicates how long the device can keep records of the locations

before offloading to a server, without data loss.

In the real-life application, the nodes also store other sensor information such as acceleration, heading, temperature, humidity, energy profiling, sampled at much higher frequencies due to their relatively low energy cost. We assume that of the 1MBytes storage, GPS traces can use up to 50KBytes, and that the sampling rate of GPS is 1 sample per minute. Each GPS sample requires at least 12 bytes storage (latitude, longitude, timestamp). For the error tolerance, we use 10 meters as it is reasonable for both animal tracking and vehicle tracking. The average compression rate at 10 meters for both datasets is used for the algorithms. For the DR algorithm, we assume it uses 39% more points than FBQS as shown in Figure 8(b) at the same tolerance.

Given the set up, the compression rate and estimated operational time without data loss for each algorithm are listed in Table II. We can see a maximum 36% improvement from FBQS over the existing methods (60 v.s. 44), and a maximum 41% improvement from BQS (62 v.s. 44).

TABLE II: Estimated Operational Time

	BQS	FBQS	BDP	BGD	DR
Compression rate	4.8%	5.0%	6.65%	6.75%	6.65%
Time (days)	62	60	45	44	45

5) *Run Time Efficiency*: We compared the run time efficiency of FBQS, BDP and BGD. 87,704 points from the empirical traces are used as the test data. The error tolerance is set to 10 meters. For BDP and BGD, to minimize the effect of the buffer size, we report their performances with different buffer sizes, as in Table III:

TABLE III: Performance Comparison with different buffer sizes

Buffer size (points)		32	64	128	256
Compression rate	FBQS	3.6%	—	—	—
	BDP	6.8%	6.7%	5.4%	4.9%
	BGD	6%	4.8%	4.6%	4.4%
Run time (ms)	FBQS	99	—	—	—
	BDP	76	101	163	292
	BGD	182	285	446	628

There are two notice-able advantages of FBQS from the comparison. Firstly, both the compression rate and the run time efficiency of FBQS algorithm are stable, independent of the buffer size setting. Secondly, it offers competitive run time efficiency while providing leading compression rate. The only case when BDP is able to outperform FBQS in run time efficiency is when the buffer is set to 32, where BDP has a far worse compression rate (89% more points).

VII. CONCLUSION

In this paper we present an online trajectory compression algorithm for resourced-constrained environments. We first propose a convex-hull bounding structure called the Bounded Quadrant System, and then show tight bounds can be derived from it so that compression decisions will be efficiently determined without actual deviation calculations.

To further reduce the time and space complexity of the BQS algorithm, a fast version of the BQS compression algorithm is

also proposed. In this version, error calculations are completely eliminated. Instead, when uncertain of the error, the fast algorithm aggressively takes a point. However due to the tight error bounded provided by the BQS, the overhead in the compression rate is minimum, making it a light-weight, efficient and effective algorithm, which is ideal for constrained computation environments.

As we establish the BQS algorithm, a discussion is also provided for the generalization and extensibility of the BQS algorithm for the 3-D space as well as for a different error metric. We have showed that such extensions are natural and straightforward. BQS' flexibility to generalize to other applications and settings is demonstrated.

To evaluate BQS, we have collected empirical data using a low-energy tracking platform called Camazotz on both animals and vehicles. To further widen the data variety, we also used synthetic dataset that is statistically representative of flying foxes' movement dynamics. In the experiments we evaluate the framework from various aspects. We examine the pruning power of the original BQS algorithm, demonstrating that the great pruning power of BQS leaves an ideal opportunity for FBQS to exploit so that further improvement on the time and space efficiencies is achieved without sacrificing much compression rate. We present the actual compression rates of BQS and fast BQS, and compare them to the results of competitive methods. Comparison of the estimated operational time with different algorithms is also presented. The actual run time is also reported.

There are a few immediate extensions to this work. The excellent performance of the BQS algorithms provides a unique opportunity to develop online and individualized smart systems for long-term tracking. For instance, merging and ageing can be used on the historical trajectory data to further reduce storage space. Individualized trajectory and waypoint discovery can also be used to facilitate advanced applications like real-time trip prediction or trip-duration estimation. Exploring the potential of a 4-D BQS could be another interesting extension to this work.

REFERENCES

- [1] R. Jurdak, P. Corke, A. Cotillon, D. Dharman, C. Crossman, and G. Salagnac, "Energy-efficient localisation: Gps duty cycling with radio ranging," *Transactions on Sensor Networks*, vol. 9, no. 2, 2013.
- [2] D. Van Krevelen and R. Poelman, "A survey of augmented reality technologies, applications and limitations," *International Journal of Virtual Reality*, vol. 9, no. 2, p. 1, 2010.
- [3] S. B. Eisenman, E. Miluzzo, N. D. Lane, R. A. Peterson, G.-S. Ahn, and A. T. Campbell, "Bikenet: A mobile sensing system for cyclist experience mapping," *TOSN*, vol. 6, no. 1, 2009.
- [4] R. Jurdak, P. Sommer, B. Kusy, N. Kottege, C. Crossman, A. Mckeown, and D. Westcott, "Camazotz: multimodal activity-based gps sampling," in *IPSN*, 2013, pp. 67–78.
- [5] M. Nagy, Z. Ákos, D. Biro, and T. Vicsek, "Hierarchical group dynamics in pigeon flocks," *Nature*, vol. 464, no. 7290, pp. 890–893, 2010.
- [6] D. H. Douglas and T. K. Peucker, *Algorithms for the Reduction of the Number of Points Required to Represent a Digitized Line or its Caricature*. John Wiley and Sons, Ltd, 2011, pp. 15–28.

- [7] J. Hershberger and J. Snoeyink, "Speeding up the douglas-peucker line-simplification algorithm," in *Proc. 5th Intl. Symp. on Spatial Data Handling*, 1992, pp. 134–143.
- [8] J. Muckell, J. Olsen, PaulW., J.-H. Hwang, C. Lawson, and S. Ravi, "Compression of trajectory data: a comprehensive evaluation and new approach," *GeoInformatica*, pp. 1–26, 2013.
- [9] E. Keogh, S. Chu, D. Hart, and M. Pazzani, "An online algorithm for segmenting time series," in *Proc. ICDM 2001*, 2001, pp. 289–296.
- [10] M. Chen, M. Xu, and P. Frnti, "A fast $o(n)$ multiresolution polygonal approximation algorithm for gps trajectory simplification," *IEEE Transactions on Image Processing*, vol. 21, no. 5, pp. 2770–2785, 2012.
- [11] C. Long, R. C.-W. Wong, and H. V. Jagadish, "Direction-preserving trajectory simplification," *Proc. VLDB Endow.*, vol. 6, no. 10, pp. 949–960, Aug. 2013.
- [12] J. Muckell, J.-H. Hwang, V. Patil, C. T. Lawson, F. Ping, and S. S. Ravi, "Squish: An online approach for gps trajectory compression," in *Proc. COM.Geo '11*. ACM, 2011, pp. 13:1–13:8.
- [13] M. Potamias, K. Patroumpas, and T. Sellis, "Sampling trajectory streams with spatiotemporal criteria," in *Scientific and Statistical Database Management, 2006. 18th International Conference on*, 2006, pp. 275–284.
- [14] G. Liu, M. Iwai, and K. Sezaki, "An online method for trajectory simplification under uncertainty of gps," in *Information and Media Technologies; VOL.8; NO.3*, 2013, pp. 665–674.
- [15] G. Trajcevski, H. Cao, P. Scheuermann, O. Wolfson, and D. Vaccaro, "On-line data reduction and the quality of history in moving objects databases," in *Proc. MobiDE '06*. ACM, 2006, pp. 19–26.
- [16] M. B. Kjergaard, J. Langdal, T. Godsk, and T. Toftkjær, "Entracked: Energy-efficient robust position tracking for mobile devices," in *Proc. MobiSys '09*. ACM, 2009, pp. 221–234.
- [17] P. S. Heckbert and M. Garland, "Survey of polygonal surface simplification algorithms," 1995.
- [18] D. E. Knuth, *The Art of Computer Programming, Volume 2 (3rd Ed.): Seminumerical Algorithms*. Boston, MA, USA: Addison-Wesley Longman Publishing Co., Inc., 1997.
- [19] J. Hightower, "SpotON: An Indoor 3D Location Sensing Technology Based on RF Signal Strength."
- [20] H. Cao, O. Wolfson, and G. Trajcevski, "Spatio-temporal data reduction with deterministic error bounds," *The VLDB Journal*, vol. 15, no. 3, pp. 211–228, Sep. 2006.
- [21] H. Risken, *The Fokker-Planck Equation: Methods of Solutions and Applications*, 2nd ed., ser. Springer Series in Synergetics. Springer, Sep. 1996.

VIII. APPENDIX: DISCUSSION AND PROOF OF THEOREMS

First we explain the purpose of splitting the space into four quadrants and the properties obtained by this setup.

- No two bounding lines will intersect with the same edge of a bounding box, and every edge will have exactly one intersection with the bounding lines, except at the corner points or on the axes.
- The angle between $l_{s,e}$ and either of the two bounding lines will be smaller than 90° ,
- Hence, any point will be bounded by the convex hull formed by the points $\{l_1, l_2, u_1, u_2, c_n, c_f\}$. No bounding convex-hulls from two adjacent BQS will overlap.

Splitting the space into four quadrants ensures that the aforementioned properties hold. Otherwise, the only case that the convex hull $l_1 l_2 c_f u_2 u_1 c_n$ may not cover all the points is when there is an edge with zero intersection from the bounding lines, as depicted in Figure 9. In this case, c_f is

c_3 , however c_2 has a greater deviation to $l_{s,e}$ than any point in $\{l_1, l_2, u_1, u_2, c_n, c_f\}$. Notice that when the system is in a single quadrant, the layout would not be a possibility.

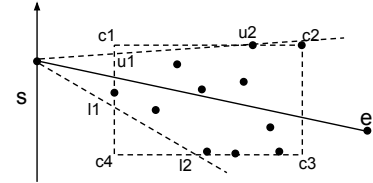


Fig. 9: Bounding system across quadrants

Next we present the proof for Theorems 5.3, 5.4, and 5.5:

a) *Proof of Theorem 5.3:* Using the first quadrant as example as shown in Figure 2, we can state there are no points in areas $\overline{c_1 u_1 u_2}$ or $\overline{c_3 l_1 l_2}$. Now we have the following properties:

- $d(u_1, l_{s,e}) \leq d^{max}(p, l_{s,e}) \leq d(u_2, l_{s,e})$: Because the angle between $l_{s,e}$ and l_{u_1, u_2} is less than or equal to 90° , if we extend $\overline{u_2 c_2}$ to intersect with $l_{s,e}$ at p_1 , the three vertices form a triangle $\overline{u_2 p_1 s}$, so the greatest distance from any point in the triangle to the edge $l_{s,e}$ would be $d(u_2, l_{s,e})$. Then because the bounding line dictates that there must be at least one point (denoted as p^u) in the line segment $\overline{u_1, u_2}$, which does not intersect with line $l_{s,e}$, we have $d(p^u, l_{s,e}) \leq \min\{d(u_1, l_{s,e}), d(u_2, l_{s,e})\}$. In this case we have $\min\{d(u_1, l_{s,e}), d(u_2, l_{s,e})\} = d(u_1, l_{s,e})$, hence we have $d(u_1, l_{s,e}) \leq d^{max}(p_i, l_{s,e}) \leq d(u_2, l_{s,e})$.
- $d(l_1, l_{s,e}) \leq d^{max}(p_i, l_{s,e}) \leq d(l_2, l_{s,e})$: proof is similar as above using the triangle $\overline{u_2 p_1 s}$. We could also see that by using $\overline{l_2 p_1 s}$ we have two triangles that together contain the convex hull $\overline{c_4 u_1 u_2 c_2 l_2 l_1}$ which bounds the points, so we have $d^{max}(p_i, l_{s,e}) \leq \max\{d^{intersection}\}$ as the upper bound. Similarly, we can have $\max\{d(u_1, l_{s,e}), d(l_1, l_{s,e})\} \leq d^{max}(p_i, l_{s,e})$ as the lower bound.
- $d^{max}(p, l_{s,e}) \geq \max(d^{corner-nf})$: This property is based on the fact that the line $l_{s,e}$ will not intersect with both edges that a corner point is on except at the corner points, while every edge must have at least one point on it. In this quadrant, c_n is c_4 and c_f is c_2 . Because there is at least one point on the edge $\overline{c_1 c_2}$, and c_2 is the closest point to $l_{s,e}$ on $\overline{c_1 c_2}$, we have $d^{max}(p, l_{s,e}) \geq d(c_2, l_{s,e})$. With an identical case of edge $\overline{c_1 c_4}$, we have $d^{max}(p, l_{s,e}) \geq \max(d^{corner-nf})$ when we combine the lower bounds.

The line $l_{s,e}$ may intersect with the bounding box in different angle and at different locations but with the properties guaranteed by the BQS, we can use the same proof for all cases.

Theorems 5.4 is proven with similar techniques. Theorem 5.5, i.e. cases in which the line $l_{s,e}$ is in a different quadrant from the bounding box, can be proven using the same proof as for Theorem 5.2.